Solar Energy Materials and Solar Cells 201 (2019) 110075

Contents lists available at ScienceDirect

Solar Energy Materials and Solar Cells

journal homepage: www.elsevier.com/locate/solmat

Thermally-induced wrinkles on PH1000/graphene composite electrode for enhanced efficiency of organic solar cells

Yang Chen[a,b], Yuan-yuan Yue[a], Shi-Rong Wang[a], Nan Zhang[a], Jing Feng[a,**], Hong-Bo Sun[a,c,*]

[a] State Key Laboratory of Integrated Optoelectronics, College of Electronic Science and Engineering, Jilin University, 2699 Qianjin Street, Changchun, 130012, People's Republic of China

[b] State Key Laboratory of Luminescence and Applications, Changchun Institute of Optics, Fine Mechanics and Physics, Chinese Academy of Sciences, Changchun, 130033, China

[c] State Key Laboratory of Precision Measurement Technology and Instruments, Department of Precision Instrument, Tsinghua University, Haidian, Beijing, 100084, People's Republic of China

ARTICLE INFO

Keywords:
graphene
Thermally-induced wrinkles
composite electrode
Organic solar cell

ABSTRACT

PH1000/graphene (Gra) composite film with thermally-induced wrinkles has been employed as an electrode in organic solar cells (OSCs) to enhance the device efficiency. The wrinkled PH1000/Gra composite electrode exhibits excellent transmittance of 88.5% at 550 nm, decreased sheet resistance of 147.5 Ω sq^{-1} and appropriate work function of ~4.9 eV compared to pristine graphene. OSCs with wrinkled composite electrode possess enhanced short circuit current (J_{SC}) compared to that of planar devices due to the wrinkles-induced enhancements in light absorption and charge collection. The power conversion efficiency (PCE) of OSCs with wrinkled composite electrode is 4.67%, which is 60% or 35% higher than that of planar devices based on the pristine graphene (2.93%) or PH1000 (3.45%) electrode, respectively. Corresponding PCE is comparable to that of the conventional ITO-based OSCs (5.08%). Even better, flexible OSCs with PH1000/Gra composite electrode exhibited excellent mechanical stability compared to ITO device. The enhanced efficiency of the OSCs demonstrates that the wrinkled PH1000/Gra composite electrode is a promising candidate for efficient and flexible optoelectronic application.

1. Introduction

In the past few decades, graphene has grown as a favorable transparent and conductive electrode (TCE) due to its unique properties compared to that of metal film, metal nanowire and carbon nanotube in optical transparency, carrier mobility, flexibility and thermal/chemical stability [1–6]. Graphene TCE has been widely applied in various optoelectronic devices such as organic light-emitting diodes [7–9], organic solar cells (OSCs) [10–12], transistors [13,14] and supercapacitors [15–17]. However, chemical vapor deposition (CVD) synthesized monolayer graphene always possesses a polycrystalline nature with grain size of several micrometers, which degrades the electrical properties of graphene film [18–21]. The sheet resistance of CVD-grown monolayer graphene transferred onto insulating substrate could reach up to 1000 Ω sq^{-1}, which is much higher than traditional indium tin oxides electrode (ITO ~15 Ω sq^{-1}) [22,23]. Besides, pristine CVD-grown graphene suffers from a low work function, which mismatched with the energy level of adjacent functional materials in optoelectronic devices [24,25]. Previous researches have reported $AuCl_3$ as p-type dopant for graphene to improve its conductivity and work function, while Au particles on graphene deteriorate the smooth surface morphology and even optical transparency [26–28].

Conducting polymer, such as poly(3,4-ethylenedioxythiophene):poly(styrenesulfonate) (PEDOT:PSS), is widely applied as anode or hole injection layer in organic optoelectronic devices due to its flexibility, high transmittance and proper work function [29–31]. Unfortunately, pristine PEDOT:PSS film exhibits low electrical conductivity because of the insulating PSS component. As a result, several methods have been applied to enhance electrical conductivity of the PEDOT:PSS film. Doping polar solvents, like dimethyl sulfoxide (DMSO), in the PEDOT:PSS could modify its features into outstretched grain size and more continuous PEDOT interconnection [32–34]. Huang et al. demonstrated that PEDOT:PSS doped with polyethylene oxide signally enhances its electrical conductivity and offers efficient

* Corresponding author. State Key Laboratory on Integrated Optoelectronics, College of Electronic Science and Engineering, Jilin University, 2699 Qianjin Street, Changchun, 130012, People's Republic of China.

** Corresponding author.

E-mail addresses: jingfeng@jlu.edu.cn (J. Feng), hbsun@tsinghua.edu.cn (H.-B. Sun).

https://doi.org/10.1016/j.solmat.2019.110075
Received 6 March 2019; Received in revised form 22 July 2019; Accepted 23 July 2019
Available online 31 July 2019

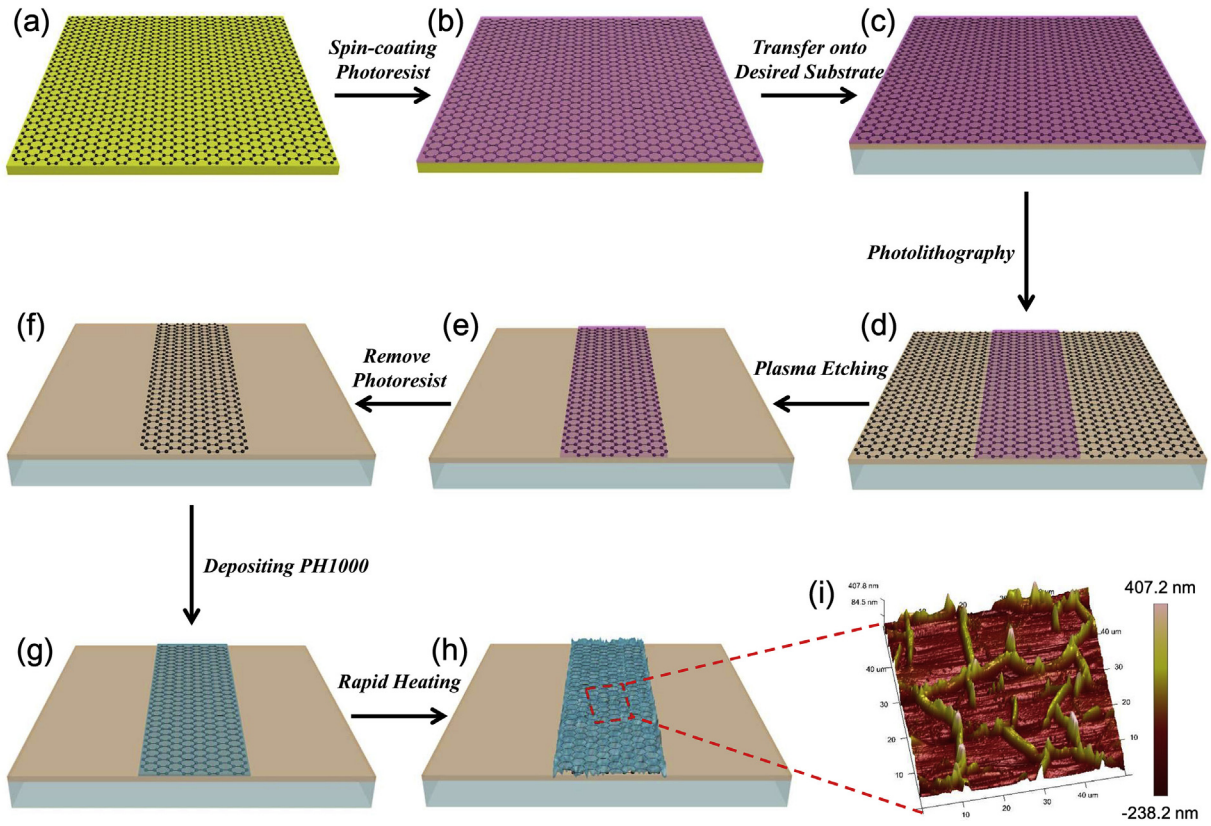

Fig. 1. The fabrication schematic diagram of patterned PH1000/Gra electrode. (a) Large area graphene film is synthesized on copper foils. (b) S1805G photoresist is spin-coated on graphene film. (c) Removing copper foils and transferring S1805G/graphene onto substrate. (d) The photolithography is applied to fabricate S1805G patterns. (e) The patterns on S1805G are transferred on to graphene by plasma etching. (f) Removing S1805G and leaving patterned graphene on substrate. (g) Depositing PH1000 polymer on patterned graphene film. (h) Formation of the wrinkled structures by a rapid heating process. (i) 3-D AFM image of wrinkled PH1000/Gra films.

carrier collection [32]. Post-treatment of PEDOT:PSS with inorganic acid results in morphology changes as well as the removal of undesired PSS from the film surface [35]. In addition, metal nanowire [36], carbon nanotube [37] and graphene [38,39] also have been combined with conducting polymer as composite electrodes to decrease the film resistance.

Herein, we have demonstrated wrinkled composite electrode of DMSO doped PEDOT:PSS (PH1000) film on monolayer graphene (PH1000/Gra) with high optical transparency and electrical conductivity. Microscale wrinkled profile of the PH1000/Gra composite film are formed on SU-8 polymer by introducing tensile strains between these layers during the rapid annealing process. Negative thermal expansion coefficient of graphene plays the key role to enlarge the tensile strains between conducting polymer and SU-8 film to obtain an interlaced and continuous wrinkled structure with heights of 200–300 nm. OSCs with wrinkled composite electrode show higher J_{SC} and PCE compared with devices based on pristine graphene or PH1000 electrodes, as well as the flat PH1000/Gra composite electrode. The increased current density of wrinkled OSCs is mainly due to the wrinkles-induced enhancements in light absorption and charge collection.

2. Experimental details

2.1. Preparation of graphene and PEDOT:PSS films

25 μm thick Cu foils (Alfa Aesar, 40365) were selected as catalytic metal substrate to synthesized monolayer graphene at 1000 °C for 50 min by a CVD system. The gas flows of methane, hydrogen and argon are 6, 10 and 100 sccm, respectively. For the transfer and pattern process of graphene, a simple S1805G-based transfer-patterned strategy is applied [8]. Firstly, graphene/Cu was covered with S1805G photoresist and Cu foils was subsequently removed by $K_2S_2O_8$ etchant. Then, S1805G/graphene was transferred onto desired substrate. Due to the photosensitive characteristic of S1805G, patterned S1805G can be obtained through specific photomask. After that, Ar plasma was applied to copy the pattern from photoresist to graphene. At the end, the S1805G coverage was dissolved by 80 °C acetone and monolayer graphene patterns was transferred onto desired substrate. Here, ~140 nm SU-8 (MicroChem Corp., 2025) was inserted between graphene and glass substrate. The SU-8 was diluted into 0.1 g ml^{-1} by cyclopentanone and spin-coated at 5000 rpm for 30 s, then post-treated under 95 °C oven for 5 min and stable UV light for 3 min, successively. PH1000 (Xi'an *p*-OLED, China) filtrated by 0.55 μm filter membrane was mixed with ethanol and DMSO at the volume of 1:1:0.1. Then, modified PH1000 was spin-coated onto patterned monolayer graphene/SU-8 films and annealing at a pre-heated 120 °C hot plate for rapid heating-up.

2.2. Materials characterization

Three dimensional depth of field microscope (OLYMPUS, OLS4100), atomic force microscope (AFM, Bruker Corporation, Dimension Icon) and scanning electron microscope (SEM, JEOL, JSM-7500F) were applied to explore the surface morphology of various samples. UV–vis spectrophotometer (SHIMADZU, UV-2550 and UV-3600) and four-probe resistance tester (RTS-5 Type, China) were applied to measure optical transmittance and sheet resistance of as-prepared electrode films, respectively. Raman spectrophotometer (HORIBA, LabRAM) measured the Raman spectra of graphene films at 532 nm laser and their work function was detected by ultraviolet photoelectron spectroscopy (UPS, PREVAC).

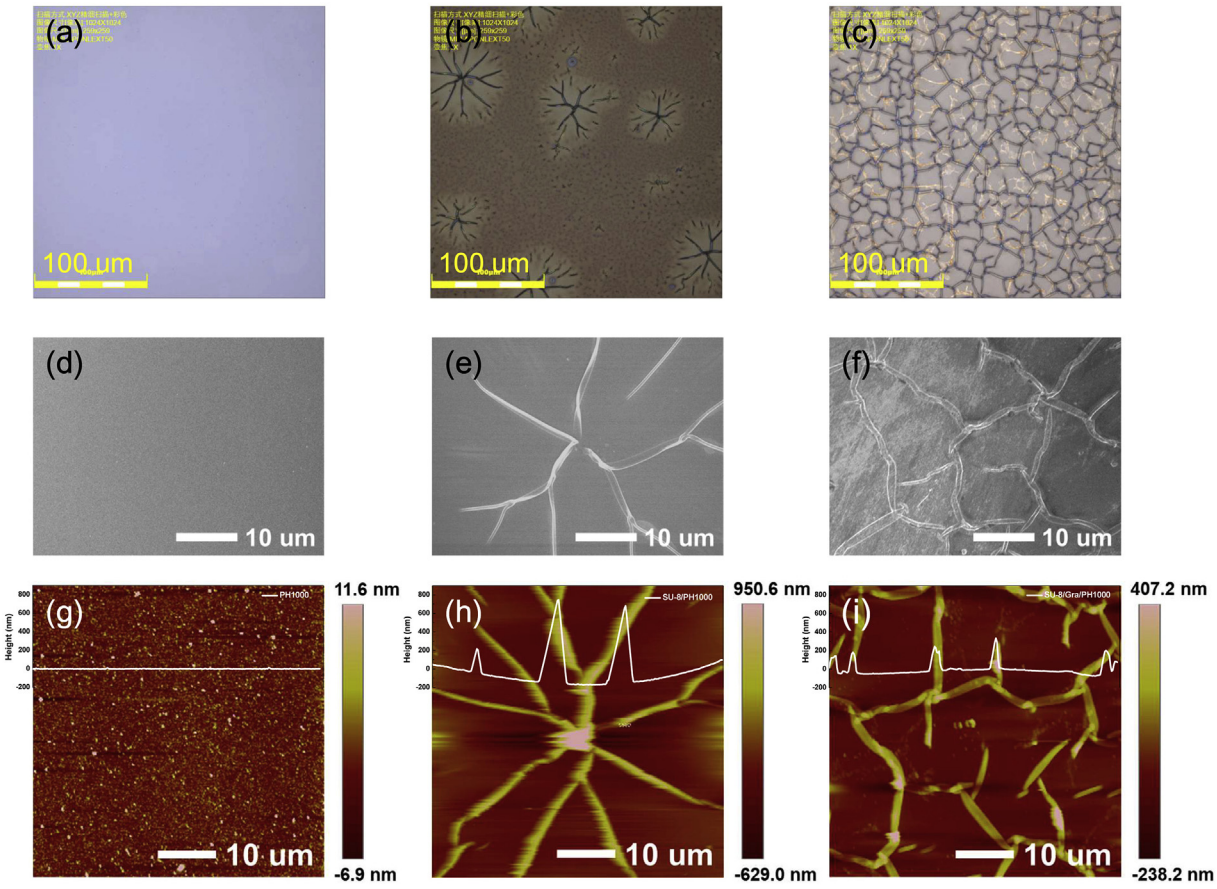

Fig. 2. (a)–(c) 3-D depth of field microscope images of PH1000 spin-coated onto glass (a), SU-8/glass (b) and graphene/SU-8/glass (c) substrates, respectively. (d)–(f) SEM images PH1000 spin-coated onto glass (d), SU-8/glass (e) and graphene/SU-8/glass (f) substrates, respectively. (g)–(i) AFM images of PH1000 spin-coated onto glass (g), SU-8/glass (h) and graphene/SU-8/glass (i) substrates, respectively.

2.3. Fabrication and measurement of OSCs

PEDOT:PSS (4083) was firstly filtrated by 0.22 μm filter membrane and mixed with isopropanol at volume of 2:1, then dilute PEDOT:PSS was deposited on the top of electrode at 3000 rpm for 30 s and annealing at 120 °C for 10 min. The annealed 4083 acts as the hole extraction layer. PCDTBT and $PC_{71}BM$ were used as the active materials with mass ratio of 1:4 in dichlorobenzene (10 mg ml^{-1} for PCDTBT), the active layer was spin-coated at 3000 rpm for 30 s and annealing at 70 °C for 1h in nitrogen condition. 2 nm Ca and 80 nm Ag were thermally evaporated as cathode in a vacuum evaporation system (FS450), creating a device active area of 0.04 cm^2. For flexible OSCs fabrication, PH1000/Gra/SU-8/NOA63 and ITO/PEN were used. Keithley 2400 was applied to measure the OSCs performance under 1 sun light simulator, the class of sunlight simulator (XES-70S1, san ei electric co.) is AAA. The light intensity was calibrated by a standard Si photodiode detector equipped with a KG-5 filter. Corresponding external quantum efficiency (EQE) spectra of device is measured by an AM 1.5 solar photon flux spectrum (Enli Technology, Taiwan).

3. Results and discussion

The schematic diagram in Fig. 1a–h shows the fabrication process of wrinkled PH1000/Gra composite electrode. Graphene grown on Cu foil was transferred and patterned on glass/SU-8 substrate by S1805G photoresist, the detailed process is presented in experimental section. Wrinkled PH1000/Gra composite film is simply fabricated by applying a rapid heating process. Fig. 1i shows the three-dimensional (3-D) AFM image of wrinkled PH1000/Gra composite film. The 3-D depth of field microscope (3-D microscope) photograph of graphic boundaries of monolayer graphene, PH1000 and PH1000/Gra composite film are shown in Figs. S1a–c, respectively. The well-defined and straight boundary line for both graphene and composite PH1000/Gra films demonstrate the accuracy of the transfer-pattern strategy. Comparing to the patterned PH1000 on glass substrate in Fig. S1b, PH1000/Gra on SU-8/glass substrate exhibits continuous and interlaced wrinkled profile. Corresponding AFM images of flat area in these electrodes are shown in Fig. S2. Both crack and wrinkle are observed in transfer-patterned monolayer graphene film (Fig. S2a). While Fig. S2c proves that PH1000 on graphene restores its surface defects thus results in continuous film morphology. The surface roughness of graphene, PH1000 and PH1000/Gra is 0.38, 0.99 and 0.97 nm, respectively. All these roughness values are much lower than that of the commercial ITO electrode (1.85 nm, Fig. S2d).

To investigate the formation of the wrinkles, PH1000 is spin-coated on glass, SU-8/glass or graphene/SU-8/glass substrates, respectively. Corresponding 3-D microscope, SEM and AFM images of PH1000 on various substrates are shown in Fig. 2. PH1000 on glass substrate (Fig. 2a, d and g) shows smooth surface morphology due to the negligible tensile strains between PH1000 and glass. While PH1000 on SU-8 modified glass (Fig. 2b, e and h) exhibits arborescent and separated wrinkled spots caused by the different thermal expansion coefficients between PH1000 and SU-8 polymers [40,41]. The inhomogeneous tensile strains in PH1000 on SU-8 during the annealing process might induce the separated wrinkled structures. Continuous and interlaced structures with typical heights of 200–300 nm and width of around 2 μm can be observed for the PH1000/Gra composite films by inserting graphene between PH1000 and SU-8 (Fig. 2c, f and i). Several works

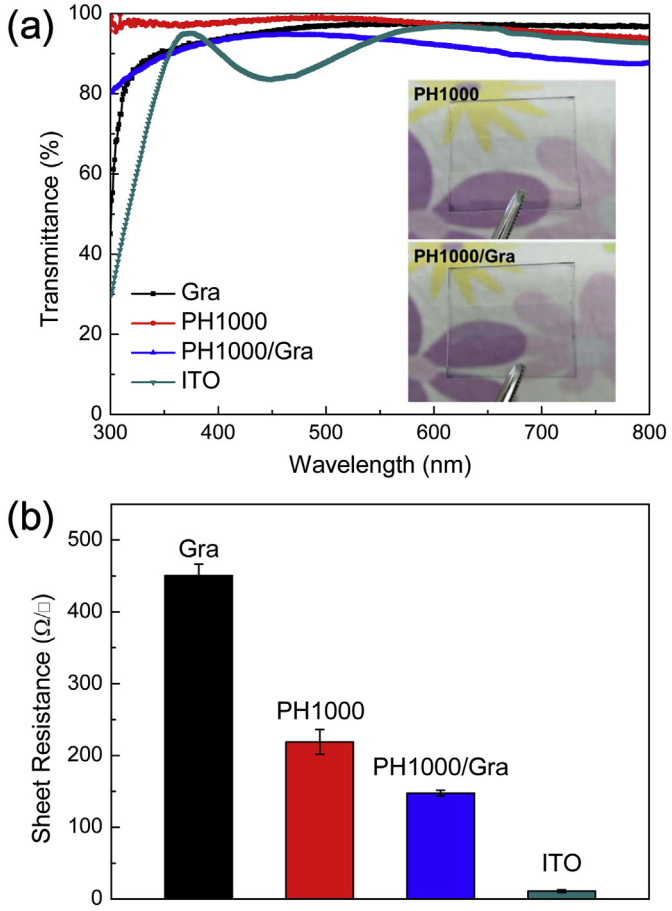

Fig. 3. (a) Transmittance spectra and (b) sheet resistance histogram of monolayer graphene, PH1000, PH1000/Gra composite film and ITO electrodes, respectively. Insets in (a) is the photograph of PH1000 and PH1000/Gra composite films.

have demonstrated that graphene possesses a negative thermal expansion coefficient, which means that graphene on substrate tends to be thermal contraction during the heating process [42–44]. In consequence, introducing the graphene between PH1000 and SU-8 films suffers stronger tensile strains resulted by the remarkable difference in the thermal expansion coefficient between these layers.

Fig. 3 shows the total transmittance spectra and sheet resistance of monolayer graphene, PH1000, PH1000/Gra and ITO electrodes, respectively. The thickness of PH1000 films on glass are ~47, ~37, ~31 and ~28 nm as the rotation speed varies from 2000 to 5000 rpm, respectively (Fig. S3). The 47 nm PH1000 film possesses a favorable transmittance of 98.4% at 550 nm and lowest average sheet resistance of 219 Ω sq^{-1} (Fig. S4). Monolayer graphene also exhibits high transmittance of above 97% at 550 nm and average sheet resistance of 450.4 Ω sq^{-1}. The total transmittance of wrinkled PH1000/Gra film can be divided into specular transmittance and scattering light due to the microscale structures. According to the total transmittance (94.1% at 550 nm), diffusive transmittance and scattering luminous flux of equipment, the haze of PH1000/Gra film can be calculated (Fig. S5) [45]. The PH1000/Gra film exhibits a maximum haze of 21.7% at the wavelength of 360 nm and lower average sheet resistance of 147.5 Ω sq^{-1} with smaller standard deviation compared to that of pristine monolayer graphene or PH1000 film. The excellent conductivity of PH1000/Gra composite film is achieved by forming new conduction paths between the grain boundaries of graphene and conductive PH1000 polymer, and each component would complement the deficiency of the other part. Therefore, PH1000/Gra with better

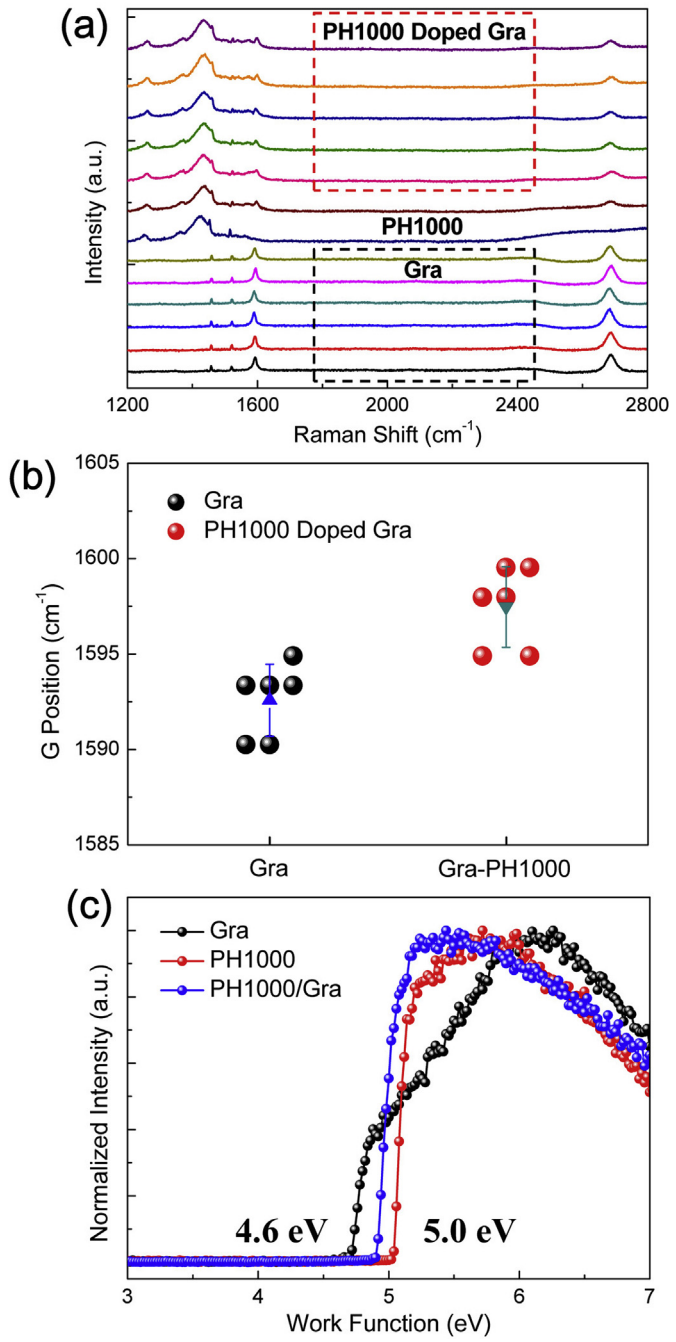

Fig. 4. (a) Raman spectra of monolayer graphene, PH1000 and PH1000 doped graphene. (b) The G band position distribution of monolayer graphene and PH1000 doped graphene. (c) UPS spectra of monolayer graphene, PH1000 conducting polymer and PH1000/Gra composite film.

conductivity would promote carrier transport by reducing the interfacial buck series resistance in OSCs thus enhance the device performance. Besides, PH1000/Gra composite electrode shows excellent mechanical stability compared to ITO (Fig. S6). After 1000 bending cycles at radius of 5 mm, the sheet resistance of PH1000/Gra composite electrode is almost unchanged, while ITO electrode dramatically increases from 15.6 Ω sq^{-1} to 1468 Ω sq^{-1}.

The Raman spectra of graphene, PH1000 and PH1000 doped graphene are shown in Fig. 4a. Six random regions are selected for universal detection of graphene and PH1000 doped graphene. The Raman spectra of pristine graphene shows an intensity ratio (I_{2D}/I_G) of around 2, demonstrating that as-prepared graphene is monolayer [8,12]. As for

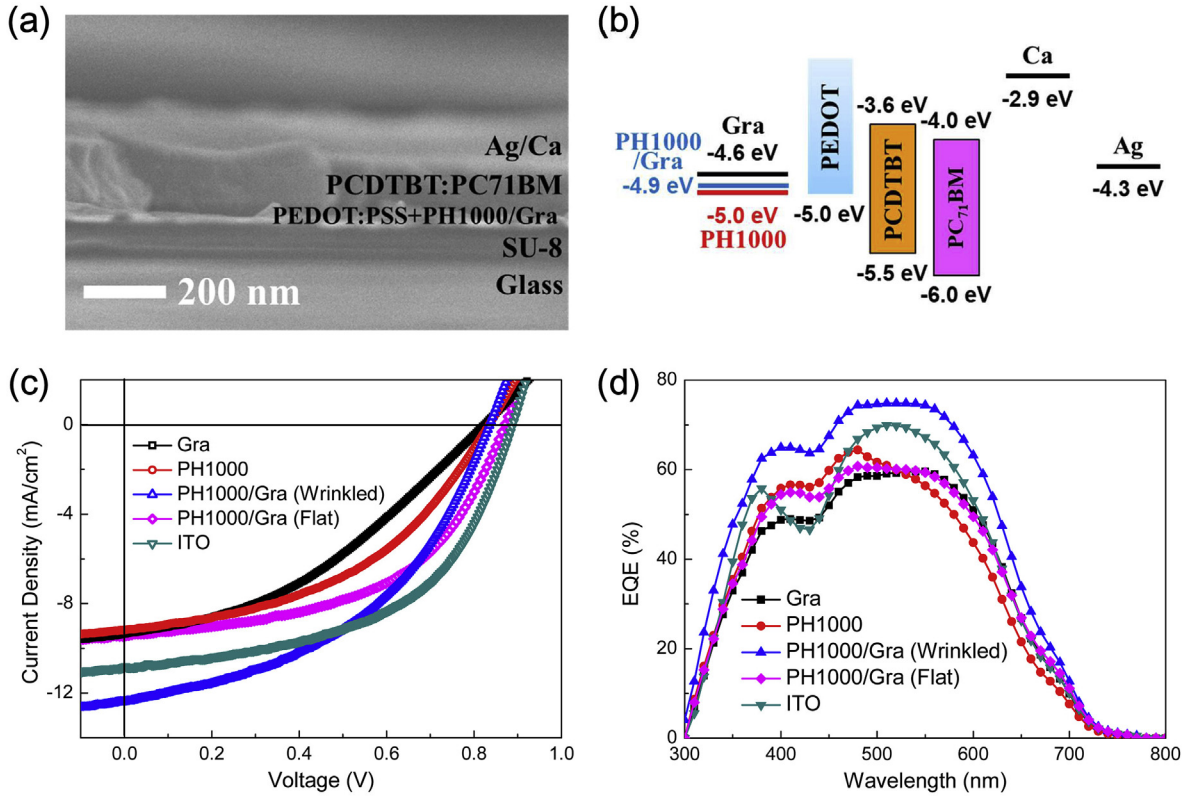

Fig. 5. (a) Cross-sectional SEM image of the OSC with PH1000/Gra composite anode. (b) The energy level distribution of as-fabricated device. (c) J-V curves and (d) EQE spectra of devices with monolayer graphene, PH1000, flat/wrinkled PH1000/Gra composite film and ITO electrodes, respectively.

Table 1
Performance summary of the device fabricated with graphene, PH1000, PH1000/Gra composite film and ITO electrodes.

Devices		V_{OC} (V)	J_{SC} (mA cm^{-2})	FF (%)	PCE (%)	EQE-J_{SC} (mA cm^{-2})
Gra	Average	0.8 (± 0.03)	9.45 (± 0.36)	35.56 (± 1.63)	2.68 (± 0.18)	9.37
	Best	0.82	9.36	37.96	2.93	
PH1000	Average	0.82 (± 0.01)	9.03 (± 1.03)	41.78 (± 5.03)	3.09 (± 0.47)	9.15
	Best	0.83	9.18	45.16	3.45	
PH1000/Gra (Flat)	Average	0.87 (± 0.01)	8.93 (± 0.35)	51.38 (± 2.28)	3.99 (± 0.27)	9.60
	Best	0.86	9.45	52.20	4.26	
PH1000/Gra (Wrinkled)	Average	0.83 (± 0.01)	12.63 (± 0.33)	42.35 (± 3.24)	4.44 (± 0.24)	11.92
	Best	0.84	12.38	45.12	4.67	
ITO	Average	0.88 (± 0.01)	10.42 (± 0.5)	51.51 (± 1.3)	4.69 (± 0.38)	10.17
	Best	0.89	10.81	52.97	5.08	

PH1000 doped graphene, the Raman spectra exhibit both signals of PH1000 and the underneath graphene. The relative intensity of the graphene signal for the composite films is lower than that of pristine graphene due to the covering of the PH1000. Besides, the G band position of graphene blue-shifts to large wave numbers, indicating a p-type doping effect for the graphene in PH1000/Gra composite film. Summarized G band position distribution of pristine graphene and PH1000 doped graphene are shown in Fig. 4b, and corresponding average G band position is located at around 1592 and 1597 cm^{-1}, respectively. Assuming that $\Delta\Omega_G = 42 \times \Delta E_F$ (cm^{-1} eV^{-1}), and the G peak shift ($\Delta\Omega_G$) value is 5 cm^{-1}, the work function for graphene doped by PH1000 is about 0.1 eV above the pristine graphene [46,47]. Fig. 4c exhibits UPS spectra of pristine monolayer graphene, individual PH1000 and PH1000/Gra composite film, corresponding work function is measured to be around 4.6, 5.0 and 4.9 eV. Compared with pristine graphene, PH1000/Gra composite electrode possesses higher work function of 4.9 eV which is matched with the energy level of PEDOT:PSS hole extraction layer.

The PH1000/Gra composite layer has been applied to the OSCs as anode, and the cross-sectional SEM image of the device structure is shown in Fig. 5a. The energy level distribution of as-fabricated device is shown in Fig. 5b. The increased work function of PH1000/Gra is benefit to the hole extraction for the use of pristine graphene as the anode in OSCs. In order to fully demonstrate the advantage of wrinkled PH1000/Gra electrode, flat PH1000/Gra film was fabricated by slowly drying the complex under room temperature for 2 h. The 3-D microscope photograph of flat PH1000/Gra film is shown in Fig. S7, and none wrinkled structures is observed. The J-V curves of the OSCs based on pristine graphene, PH1000, flat/wrinkled PH1000/Gra and ITO are exhibited in Fig. 5c, and Table 1 summarizes the detailed device parameters. Four devices of each sample are employed to evaluate the uncertainties and distribution for their general performance. The best performance of devices with pristine monolayer graphene and PH1000 electrodes possess the PCE of 2.93% and 3.45%, respectively. The higher PCE of PH1000 based device mainly originates from the enhanced fill factor (FF) due to its higher conductivity and work function compared to that of pristine graphene. OSCs based on flat PH1000/Gra film exhibit a best PCE of 4.26%, which is mainly originated from its

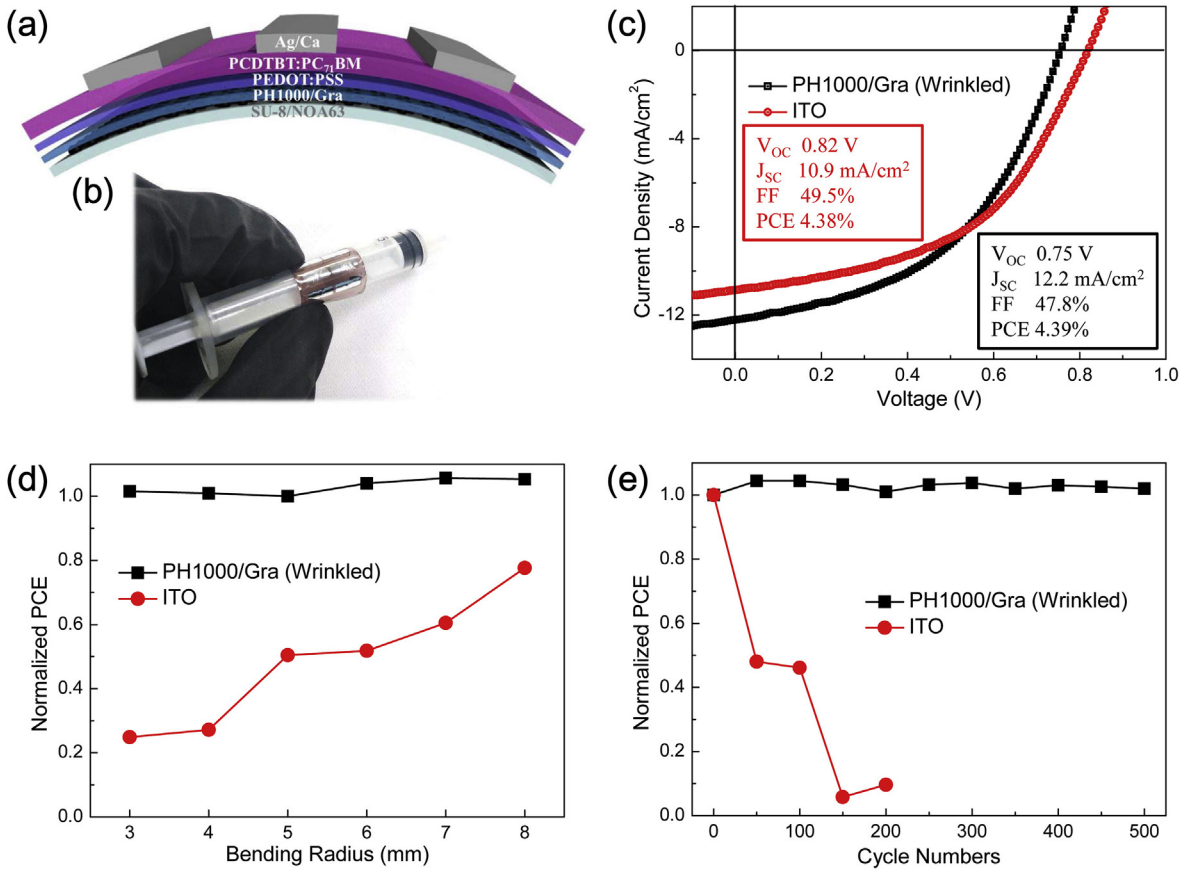

Fig. 6. (a) Device structure and (b) photograph of flexible OSCs based on wrinkled PH1000/Gra composite electrode. (c) J-V curves of flexible OSCs with wrinkled PH1000/Gra and ITO electrodes. Normalized PCE of flexible OSCs in bending test with different (d) bending radius and (e) bending cycles.

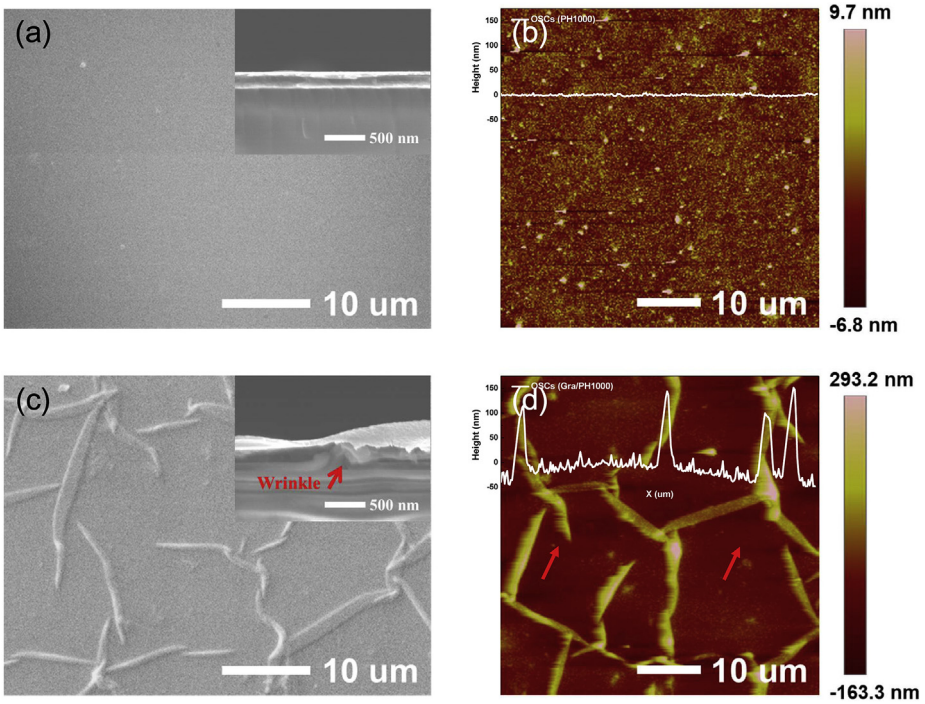

Fig. 7. Top surface profiles of the OSCs. SEM (a) and AFM (b) images of the OSCs based on the flat PH1000 electrodes. SEM (c) and AFM (d) images of the OSCs based on the wrinkled PH1000/Gra electrodes. Insets in (a) and (c) are the cross-sectional SEM images of the corresponding devices.

better FF. As for wrinkled PH1000/Gra composite electrode, the device exhibits a much higher PCE of 4.67%, which is comparable to ITO-based devices (5.08%). Especially, the device with wrinkled PH1000/Gra composite electrode exhibits the highest J_{SC} of 12.38 mA cm^{-2} compared to all these reference devices including that of flat PH1000/Gra electrode. The calculated J_{SC} from the EQE spectra is 9.37, 9.15, 9.60, 11.92 and 10.17 mA cm^{-2}, respectively, which exhibits consistent trend with the data extracted from the measured J-V characteristics (Table 1). The ITO-based device exhibits relatively low EQE values at the range of 380–500 nm, which is originated from the absorption of the ITO at this wavelength region (Fig. 3a).

In order to fully demonstrate the advantage of PH1000/Gra composite electrode, flexible OSCs are fabricated on NOA63 or PEN substrates (Fig. 6a and b). Consistent with above rigid devices, flexible OSCs based on wrinkled PH1000/Gra composite electrode possess higher J_{SC} of 12.2 mA cm^{-2} compared to that of ITO (10.9 mA cm^{-2}). The best PCE of flexible device with wrinkled composite electrode reaches to 4.39%, slightly higher than 4.38% of ITO device (Fig. 6c). Fig. 6d and e show the bending performance of flexible OSCs under different bending radius and cycle, respectively. Flexible OSCs based on wrinkled PH1000/Gra composite electrode maintain most of its initial PCE with the bending radius varied from 3 mm to 8 mm, as well as 500 bending cycles. The excellent mechanical stability of PH1000/Gra composite electrode proves its great potential in flexible optoelectronic devices. As comparison, the PCE of flexible OSCs with ITO electrode dramatically decreases to 24.9% of its initial PCE under the bending radius of 3 mm. Besides, ITO based device maintains only 5.8% of the PCE after 150 bending cycles due to the inevitable brittleness of ITO electrode.

The enhanced J_{SC} for the PH1000/Gra based OSCs can be attributed to the enhanced light scattering and charge collection compared to the planar devices induced by the wrinkled profile of the composite anode. The SEM and AFM images of the surface profile on the top of the OSCs are shown in Fig. 7. The SEM image of top device morphology in Fig. 7c confirms the transfer of the wrinkled profile from the bottom to the top electrodes. The top cathode still maintains wrinkled structures with heights of 100–150 nm (Fig. 7d). Light incident on wrinkled top electrode would be scattered or reflected at various angle, and results in enhanced light absorption by increasing its propagation length [40,48]. On the other hand, the wrinkled profile of the PH1000/Gra composite electrodes is benefit to the charge collection. Incorporating PH1000/Gra composite electrode into the active layer results in not only increased contact area between the electrode and the active layer, but also shortened pathway of the carries from the active layer to the electrode. Enhanced light absorption and charge collection are both contributed to the enhanced J_{SC} of device with wrinkled PH1000/Gra composite electrode, and results in efficient organic cells with higher PCE. The proposed fabrication process of wrinkled devices has a great potential for flexible organic optoelectronics due to its low-temperature and simple processing.

4. Conclusions

In conclusion, wrinkled PH1000/Gra composite electrode is fabricated on SU-8 polymer due to the different thermal expansion coefficient between these layers. Negative thermal expansion coefficient of graphene enlarges the tensile strains between PH1000 and SU-8 film thus inducing interlaced and continuous wrinkled structures. OSCs based on the wrinkled PH1000/Gra composite electrode exhibit enhanced J_{SC} due to the enhanced light absorption and charge collection induced by the wrinkled profile. The PCE of the wrinkled OSCs is 4.67%, which achieves 60% or 35% enhancement compared to the OSCs based on the pristine monolayer graphene (2.93%) or PH1000 (3.45%) electrode, respectively. Moreover, flexible OSCs based on wrinkled PH1000/Gra composite electrode possess slightly higher PCE and excellent mechanical stability compared to that of ITO electrode. Therefore, the wrinkled PH1000/Gra composite electrode is a promising electrode candidate for efficient and flexible optoelectronic devices.

Acknowledgements

This work was supported by the National Key Research and Development Program of China and National Natural Science Foundation of China (NSFC) under Grants # 2017YFB0404500, #61825402, #61675085, #61705075, #61605056 and 61805096.

Appendix A. Supplementary data

Supplementary data to this article can be found online at https://doi.org/10.1016/j.solmat.2019.110075.

References

[1] H.B. Jiang, Y.L. Zhang, Y. Liu, X.F. Fu, Y.F. Li, Y.Q. Liu, C.H. Li, H.B. Sun, Bioinspired few-layer graphene prepared by chemical vapor deposition on femtosecond laser-structured Cu foil, Laser Photon. Rev. 10 (2016) 441–450.
[2] B.B. Zeng, Z.Q. Huang, A. Singh, Y. Yao, A.K. Azad, A.D. Mohite, A.J. Taylor, D.R. Smith, H.T. Chen, Hybrid graphene metasurfaces for high-speed mid-infrared light modulation and single-pixel imaging, Light Sci. Appl. (7) (2018) 51.
[3] Y.B. Zhu, Z.Y. Li, Z. Hao, C. DiMarco, P. Maturavongsadit, Y.F. Hao, M. Lu, A. Stein, Q. Wang, J. Hone, N.F. Yu, Q. Lin, Optical conductivity-based ultrasensitive mid-infrared biosensing on a hybrid metasurface, Light Sci. Appl. 7 (2018) 67.
[4] S.V. Morozov, K.S. Novoselov, M.I. Katsnelson, F. Schedin, D.C. Elias, J.A. Jaszczak, A.K. Geim, Giant intrinsic carrier mobilities in graphene and its bilayer, Phys. Rev. Lett. 100 (2008) 016602.
[5] K.S. Novoselov, A.K. Geim, S.V. Morozov, D. Jiang, Y. Zhang, S.V. Dubonos, I.V. Grigorieva, A.A. Firsov, Electric field effect in atomically thin carbon films, Science (306) (2004) 666–669.
[6] A.A. Balandin, S. Ghosh, W.Z. Bao, I. Calizo, D. Teweldebrhan, F. Miao, C.N. Lau, Superior thermal conductivity of single-layer graphene, Nano Lett. (8) (2008) 902–907.
[7] Y.G. Bi, J. Feng, Y.F. Li, Y.L. Zhang, Y.S. Liu, L. Chen, Y.F. Liu, L. Guo, S. Wei, H.B. Sun, Arbitrary shape designable microscale organic light-emitting devices by using femtosecond laser reduced graphene oxide as a patterned electrode, ACS Photonics (1) (2014) 690–695.
[8] Y. Chen, N. Zhang, Y.F. Li, Y.,G. Bi, Y.Y. Yue, J. Feng, H.B. Sun, Microscale-patterned graphene electrodes for organic light-emitting devices by a simple patterning strategy, Adv. Optical Mater. (2018) 1701348.
[9] T.H. Han, Y. Lee, M.R. Choi, S.H. Woo, S.H. Bae, B.H. Hong, J.H. Ahn, T.W. Lee, Extremely efficient flexible organic light-emitting diodes with modified graphene anode, Nature Photon (6) (2012) 105–110.
[10] X. Chen, B.H. Jia, Y.N. Zhang, M. Gu, Exceeding the limit of plasmonic light trapping in textured screen-printed solar cells using Al nanoparticles and wrinkle-like graphene sheets, Light Sci. Appl. (2) (2013) e92.
[11] S. Jung, J. Lee, J. Seo, U. Kim, Y. Choi, H. Park, Development of annealing-free, solution-processable inverted organic solar cells with n-doped graphene electrodes using zinc oxide nanoparticles, Nano Lett. (18) (2018) 1337–1343.
[12] Y. Chen, J. Feng, F.X. Dong, Y.F. Li, Y.G. Bi, Y.Y. Yue, H.B. Sun, A two-step thermal annealing and HNO_3 doping treatment for graphene electrode and its application in small-molecule organic solar cells, Org, Electron (38) (2016) 35–41.
[13] W.H. Lee, J. Park, S.H. Sim, S.B. Jo, K.S. Kim, B.H. Hong, K. Cho, Transparent flexible organic transistors based on monolayer graphene electrodes on plastic, Adv. Mater. (23) (2011) 1752–1756.
[14] Y.S. Chen, Y.F. Xu, K. Zhao, X.J. Wan, J.C. Deng, W.B. Yan, Towards flexible all-carbon electronics: flexible organic field-effect transistors and inverter circuits using solution-processed all-graphene source/drain/gate electrodes, Nano Res (3) (2010) 714–721.
[15] X.Y. Zhang, S.H. Sun, X.J. Sun, Y.R. Zhao, L. Chen, Y. Yang, W. Lü, D.B. Li, Plasma-induced, nitrogen-doped graphene-based aerogels for high-performance supercapacitors, Light Sci. Appl. (5) (2016) e16130.
[16] D.D. Nguyen, P.Y. Hsieh, M.T. Tsai, C.Y. Lee, N.H. Tai, B.D. To, D.T. Vu, C.C. Hsu, Hollow few-layer graphene-based structures from parafilm waste for flexible transparent supercapacitors and oil spill cleanup, ACS Appl. Mater. Interfaces 9 (2017) 40645–40654.
[17] Z. Weng, Y. Su, D.W. Wang, F. Li, J. Du, H.M. Cheng, Graphene–cellulose paper flexible supercapacitors, Adv. Energy Mater. (1) (2011) 917–922.
[18] I. Vlassiouk, M. Regmi, P. Fulvio, S. Dai, P. Datskos, G. Eres, S. Smirnov, Role of Hydrogen in chemical vapor deposition growth of large single-crystal graphene, ACS Nano 5 (2011) 6069–6076.
[19] J. Zhang, P.A. Hu, X.N. Wang, Z.L. Wang, D.Q. Liu, B. Yang, W.W. Cao, CVD growth of large area and uniform graphene on tilted copper foil for high performance flexible transparent conductive film, J. Mater. Chem. (22) (2012) 18283–18290.
[20] W.H. Park, I. Jo, B.H. Hong, H. Cheong, Controlling the ripple density and heights: a new way to improve the electrical performance of CVD-grown graphene, Nanoscale (8) (2016) 9822–9827.

[21] Y.F. Hao, M.S. Bharathi, L. Wang, Y.Y. Liu, H. Chen, S. Nie, X.H. Wang, H. Chou, C. Tan, B. Fallahazad, H. Ramanarayan, C.W. Magnuson, E. Tutuc, B.I. Yakobson, K.F. McCarty, Y.W. Zhang, P. Kim, J. Hone, L. Colombo, R.S. Ruoff, The role of surface oxygen in the growth of large single-crystal graphene on copper, Science (342) (2013) 720–723.
[22] L.H. Liu, W.J. Shang, C. Han, Q. Zhang, Y. Yao, X.Q. Ma, M.H. Wang, H.T. Yu, Y. Duan, J. Sun, S.F. Chen, W. Huang, Two-in-one method for graphene transfer: simplified fabrication process for organic light-emitting diodes, ACS Appl. Mater. Interfaces (10) (2018) 7289–7295.
[23] L. Yan, Y. Zhang, X.Y. Zhang, J. Zhao, Y. Wang, T.Q. Zhang, Y.H. Jiang, W.Z. Gao, J.Z. Yin, J. Zhao, W.W. Yu, Single layer graphene electrodes for quantum dot-light emitting diodes, Nanotechnology (26) (2015) 135201.
[24] S.J. Kwon, T.H. Han, Y.H. Kim, T. Ahmed, H.K. Seo, H. Kim, D.J. Kim, W.T. Xu, B.H. Hong, J.X. Zhu, T.W. Lee, Solution-processed n-type graphene doping for cathode in inverted polymer light-emitting diodes, ACS Appl. Mater. Interfaces 10 (2018) 4874–4881.
[25] D. Kim, D. Lee, Y. Lee, D.Y. Jeon, Work-function engineering of graphene anode by Bis(trifluoromethanesulfonyl)amide doping for efficient polymer light-emitting diodes, Adv. Funct. Mater. (23) (2013) 5049–5055.
[26] K.C. Kwon, B.J. Kim, J.L. Lee, S.Y. Kim, Effect of anions in Au complexes on doping and degradation of graphene, J. Mater. Chem. C 1 (2013) 2463–2469.
[27] K.W. Kim, W. Song, M.W. Jung, M.A. Kang, S.Y. Kwon, S. Myung, J. Lim, S.S. Lee, K.S. An, Au doping effect on chemically-exfoliated graphene and graphene grown via chemical vapor deposition, Carbon (82) (2015) 96–102.
[28] S.J. Kwon, T.H. Han, T.Y. Ko, N.N. Li, Y. Kim, D.J. Kim, S.H. Bae, Y. Yang, B.H. Hong, K.S. Kim, S. Ryu, T.W. Lee, Extremely stable graphene electrodes doped with macromolecular acid, Nat. Commun. (9) (2018) 2037.
[29] S.K. Hau, H.L. Yip, J.Y. Zou, A.K.-Y. Jen, Indium tin oxide-free semi-transparent inverted polymer solar cells using conducting polymer as both bottom and top electrodes, Org. Electron. (10) (2009) 1401–1407.
[30] D. Yin, N.R. Jiang, Y.F. Liu, X.L. Zhang, A.W. Li, J. Feng, H.B. Sun, Mechanically robust stretchable organic optoelectronic devices built using a simple and universal stencil-pattern transferring technology, Light Sci. Appl. (7) (2018) 35.
[31] J. Feng, Y.F. Liu, Y.G. Bi, H.B. Sun, Light manipulation in organic light-emitting devices by integrating micro/nano patterns, Laser Photon. Rev. (2017) 1600145.
[32] X. Huang, K. Wang, C. Yi, T.Y. Meng, X. Gong, Efficient perovskite hybrid solar cells by highly electrical conductive PEDOT:PSS hole transport layer, Adv. Energy Mater. (6) (2016) 1501773.
[33] T.R. Chou, S.H. Chen, Y.T. Chiang, Y.T. Lin, C.Y. Chao, Highly conductive PEDOT:PSS films by posttreatment with dimethyl sulfoxide for ITO-free liquid crystal display, J. Mater. Chem. C (3) (2015) 3760–3766.
[34] X.Q. Zhang, J. Wu, J.T. Wang, J. Zhang, Q.Q. Yang, Y.Y. Fu, Z.Y. Xie, Highly conductive PEDOT:PSS transparent electrode prepared by a post-spin-rinsing method for efficient ITO-free polymer solar cells, Sol. Energy Mater. Sol. Cells 144 (2016) 143–149.
[35] Y.J. Xia, K. Sun, J.Y. Ouyang, Solution-processed metallic conducting polymer films as transparent electrode of optoelectronic devices, Adv. Mater. (24) (2012) 2436–2440.
[36] Y.S. Liu, J. Feng, X.L. Ou, H.F. Cui, M. Xu, H.B. Sun, Ultrasmooth, highly conductive and transparent PEDOT:PSS/silver nanowire composite electrode for flexible organic light-emitting devices, Org. Electron. (31) (2016) 247–252.
[37] J. Chen, Y. Liu, A.I. Minett, C. Lynam, J.Z. Wang, G.G. Wallace, Flexible, aligned carbon nanotube/conducting polymer electrodes for a lithium-ion battery, Chem. Mater. (19) (2007) 3595–3597.
[38] Y.F. Xu, Y. Wang, J.J. Liang, Y. Huang, Y.F. Ma, X.J. Wan, Y.S. Chen, A hybrid material of graphene and Poly (3,4-ethyldioxythiophene) with high conductivity, flexibility, and transparency, Nano Res (2) (2009) 343–348.
[39] H. Park, Y. Shia, J. Kong, Application of solvent modified PEDOT:PSS to graphene electrodes in organic solar cells, Nanoscale (5) (2013) 8934–8939.
[40] S.Y. Ryu, J.H. Seo, H. Hafeez, M. Song, J.Y. Shin, D.H. Kim, Y.C. Jung, C.S. Kim, Effects of the wrinkle structure and flat structure formed during static low-temperature annealing of ZnO on the performance of inverted polymer solar cells, J. Phys. Chem. C 121 (2017) 9191–9201.
[41] S.S. Yoo, G.H. Choi, W. Lee, J. Park, G.R. Yi, D.Y. Ryu, P.J. Yoo, Cumulative energy analysis of thermally-induced surface wrinkling of heterogeneously multilayered thin films, Soft Matter (14) (2018) 704–710.
[42] Y.F. Hu, J.P. Chen, B. Wang, On the intrinsic ripples and negative thermal expansion of graphene, Carbon (95) (2015) 239–249.
[43] Y. Magnin, G.D. Förster, F. Rabilloud, F. Calvo, A. Zappelli, C. Bichara, Thermal expansion of free-standing graphene: benchmarking semi-empirical potentials, J. Phys. Condens. Matter (26) (2014) 185401.
[44] D. Yoon, Y.W. Son, H. Cheong, Negative thermal expansion coefficient of graphene measured by Raman spectroscopy, Nano Lett. (11) (2011) 3227–3231.
[45] Y.K. Sun, F.S. Yi, Y.G. Bi, J. Feng, Spontaneously formed random corrugations for efficient light extraction enhancement in flexible organic light-emitting devices, Org. Electron. (65) (2019) 91–95.
[46] C.F. Chen, C.H. Park, B.W. Boudouris, J. Horng, B.S. Geng, C. Girit, A. Zettl, M.F. Crommie, R.A. Segalman, S.G. Louie, F. Wang, Controlling inelastic light scattering quantum pathways in graphene, Nature (471) (2011) 617–620.
[47] N. Li, S. Oida, G.S. Tulevsk, S.J. Han, J.B. Hannon, D.K. Sadana, T.C. Chen, Efficient and bright organic light-emitting diodes on single-layer graphene electrodes, Nature Commun (4) (2013) 2294.
[48] I.Y.Y. Bu, Self-assembled, wrinkled zinc oxide for enhanced solar cell performances, Mater. Lett. (122) (2014) 55–57.